Disponible en www.hormigonyacero.com
Hormigón y Acero, 2025
https://doi.org/10.33586/hya.2025.4130

ARTÍCULO EN AVANCE ON LINE

Comparison of code approaches for the SLS design of GFRP reinforced concrete flexural members

Lluís Torres, Cristina Barris, Eva Oller , Marta Baena

DOI: https://doi.org/10.33586/hya.2025.4130

Para ser publicado en: *Hormigón y Acero*

Por favor, el presente artículo debe ser citado así:
Torres, L., Barris, C., Oller, E., & Baena, M. (2025) Comparison of code approaches for the SLS design of GFRP reinforced concrete flexural members, *Hormigón y acero,* https://doi.org/10.33586/hya.2025.4130

Comparison of code approaches for the SLS design of GFRP reinforced concrete flexural members

Lluís Torres[(1)], Cristina Barris[(1*)], Eva Oller[(2)] , Marta Baena[(1)]

[(1)]Department of Mechanical Engineering and Industrial Construction, Universitat de Girona

[(2)]Department of Civil and Environmental Engineering, Universitat Politècnica de Catalunya

[(*)] Corresponding author

Abstract

When Fibre Reinforced Polymer (FRP) bars are used as embedded reinforcement in concrete structures, serviceability behaviour often governs the design due to the lower modulus of elasticity of FRPs compared to conventional steel. While many design principles for steel-reinforced concrete remain applicable, the distinct mechanical and bond properties of FRPs require special consideration. In recent years, several international codes and guidelines have been updated or newly issued to address FRP reinforcement.

This paper presents a comparative analysis of the main aspects and provisions for serviceability limit state (SLS) design of Glass FRP (GFRP) reinforced concrete flexural members included in Eurocode 2 (2023), fib Model Code 2020 and ACI440.11-22. Stress limitation, crack width and deflections are carefully reviewed, and a design example is included, where the effects of different assumptions and limitations among codes are analysed and discussed.

Keywords: Embedded FRP reinforcement, Flexural members, Design codes, Serviceability

Resumen

El comportamiento en servicio suele determinar el diseño de las estructuras de hormigón con armadura embebida de polímeros reforzados con fibras (FRP) debido a su menor módulo de elasticidad en comparación con el acero convencional. Si bien muchos principios de diseño para el hormigón armado con barras de acero siguen siendo aplicables, las características mecánicas y de adherencia de los FRPs requieren una consideración especial. En los últimos años, se han actualizado o publicado diversos códigos y guías de diseño internacionales para el refuerzo con armaduras de FRP.

Este artículo presenta un análisis comparativo de los principales aspectos y disposiciones para el diseño en estado límite de servicio (ELS) de elementos a flexión de hormigón armados con barras de polímeros reforzados con fibras de vidrio (GFRP), incluidos en el Eurocódigo 2 (2023), el Código Modelo fib 2020 y ACI440.11-22. Se revisan en detalle la limitación de tensiones, el ancho de fisura y la flecha, y se incluye un ejemplo de diseño donde se analizan y discuten los efectos de los diferentes enfoques y limitaciones entre códigos.

Palabras clave: Armadura de FRP embebida, Elementos a flexión, Códigos de diseño, Comportamiento en servicio.

1. Introduction

Fibre reinforced polymer (FRP) bars have emerged as an alternative to conventional reinforcement in reinforced concrete structures (RC) exposed to environments likely to cause

corrosion in steel reinforcement. Likewise, FRP reinforcement has demonstrated its suitability for applications requiring magnetic neutrality, or good cuttability, as for example for diaphragm walls [1-3]. Among the several types of fibres used in manufacturing the FRPs, the glass-FRP (GFRP) reinforcement has been the most used as embedded reinforcement for RC, due to the good combination of properties and cost.

Although design recommendations for FRP reinforcement were already introduced in the 1990s in Japan [4,5], it has been in the last years when a major development of codes and guidelines has been carried out. Among them, the American Concrete Institute recently published the ACI440.11-22 code for structural concrete reinforced with GFRP [6], after the publication of some previous documents in the form of guidelines [3,7]. Likewise, the fib Model Code 2020 [8] has also incorporated provisions for FRP RC design, after having introduced the FRP reinforcement in the previous fib Model Code 2010 [9]. And even more recently, the FRP RC has been introduced in the new Eurocode 2 (EN 1992-1-1:2023) in the informative Annex R [10]. In addition to these documents, there are also codes and recommendations available in other countries as for example Italy, Canada, France or Japan [11-15].

These codes and guidelines are generally based on the same principles as for conventional steel RC, although they present some modifications to accommodate the specific properties of FRPs. It is worth to mention their linear elastic behaviour up to failure, high tensile strength combined with low modulus of elasticity [16-19], and reduction of resistant capacity under sustained stresses (creep rupture) [2,3]. Additionally, there might be high variability of mechanical properties and surface treatment among the available products, due to current lack of general standardization. The existing codes for FRP RC tend to follow similar procedures to those stablished in the corresponding code of the promoting entity for steel RC. This leads to some differences among them that mainly affect design framework, calculation models, material properties to be used, and limit values of the relevant parameters to be controlled in the design. Consequently, despite that the concepts are similar, partial or global results of the design process may present differences.

This paper presents and compares the main aspects and provisions for serviceability limit state (SLS) design of GFRP RC flexural members included in current recent codes. Three of them have been selected due to their relevance at the international level: Eurocode 2 (EC2) [10], fib Model Code 2020 (MC2020) [8] and ACI440.11-22 (ACI440.11) [6]. A detailed presentation of the design methodology for control of stresses, crack width and deflections is carried out, including a design example in which the partial and global results of the design process are presented and discussed.

2. FRP mechanical properties for design

As mentioned, FRP reinforcement presents some significant differences with respect to conventional steel reinforcement. Differently from steel, FRP shows a linear elastic stress-strain behaviour up to failure. In general, the tensile strength of available products is higher than that of steel reinforcement, however, their modulus of elasticity is lower (mainly for GFRP). Consequently, these materials may present high deformability with strong incidence on the serviceability behaviour of the structure [20]. Another relevant difference is that FRP materials subjected to sustained stresses, jointly with the influence of the exposure environment, may fail due to creep rupture with a lower strength than that of the short-term value [2,3,6,8].

Material properties to be considered in design are generally defined in codes where guidance is given to obtain the corresponding values either analytically or experimentally. In terms of strength, the tensile creep rupture strength at 100 years in the relevant exposure environment is the parameter taken as a reference in both EC2 ($f_{ftk,100a}$) and MC2020 ($f_{fk,100a}$), while the long-term limit for sustained stresses in ACI440.11 was based on a service life of 114 years [21].

According to EC2, the tensile design strength, f_{ftd}, is obtained from the long-term strength, $f_{ftk,100a}$, divided by a material partial factor γ_{FRP} (1.5 for ULS persistent and transient and 1.0 for SLS):

$$f_{ftd} = \frac{f_{ftk,100a}}{\gamma_{FRP}} \tag{1}$$

EC2 allows directly obtaining the long-term strength for any specific rebar from experimental tests. In that sense, the European Assessment Document EAD 260023-00-0301 for carbon, glass, basalt and aramid FRP bars as reinforcement of structural elements [22] provides procedures based on ISO 10406-1 [23] to assess the influence of sustained loads on the performance of FRP bars commonly used as tensile reinforcement in RC structures.

In absence of data from tests, $f_{ftk,100a}$ can be conservatively evaluated by multiplying the characteristic short-term strength, f_{ftk0}, by several reducing factors:

$$f_{ftk,100a} = C_t \cdot C_c \cdot C_e \cdot f_{ftk0} \tag{2}$$

where C_t considers the temperature effects (1.0 for indoor and underground environments, 0.8 for outdoor members if heating through solar radiation cannot be excluded), C_c represents the effect of sustained load on the strength under short-term load (0.35 for GFRP reinforcement and 0.8 for CFRP reinforcement), and C_e accounts for the effect of ageing (taken as 0.7). The use of these coefficients may provide substantially low values of $f_{ftk,100a}$, as can be seen for example for a case of ULS (γ_{FRP} = 1.5) with outdoor exposure (C_t = 0.8), and GFRP reinforcement (C_c = 0.35) in which f_{ftd} would attain a value of $0.13 f_{tk0}$. Additionally, according to EC2 the FRP reinforcement must have a modulus of elasticity $E_{fR} \geq 40000$ MPa and a ratio of $f_{ftk,100a} / E_{fR} \geq 0.005$.

A schematic representation of the stress-strain behaviour and relevant parameters is shown in Figure 1.

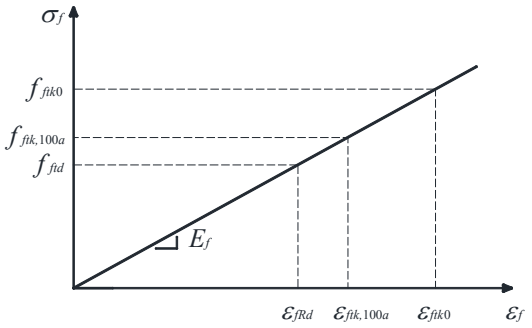

Figure 1. FRP stress-strain behaviour [10].

In MC2020 a different value is defined for the tensile design strength of FRP reinforcement to be used in ULS verifications:

$$f_{fd} = min\left\{\eta \frac{f_{fk}}{\gamma_f}; \frac{f_{fk,100a}}{\gamma_f} \frac{\gamma_G \cdot G + \gamma_Q \cdot Q}{G + \psi_2 \cdot Q}\right\} \tag{3}$$

in which the term corresponding to the long-term strength (i.e. creep rupture) is increased according to the ratio between the design factored load and the quasi-permanent load. Additionally, the design value of the stress limit for FRP creep rupture under SLS is given by:

$$\sigma_{f,creep,\,Rd} = \frac{\eta_e \cdot f_{fk,100a}}{\gamma_f} \tag{4}$$

where $f_{fk,100a}$ is the characteristic value of creep rupture strength; $\eta_e$is an environmental factor (a typical value of 0.85 is proposed); $\gamma_G \cdot G + \gamma_Q \cdot Q$ and $G + \psi_2 \cdot Q$ are the ULS and quasi-

permanent combinations, respectively; and γ_f is a material partial factor equal to 1.3 for ULS and 1.0 for SLS.

On the other hand, in ACI440.11 the design tensile strength, f_{fu}, is defined by:

$$f_{fu} = C_E \cdot f_{fu}^* \tag{5}$$

where f_{fu}^* is the guaranteed tensile strength and C_E is an environmental reduction factor taken as 0.85. In this case, the limit value for sustained stresses in GFRP bars is $0.30f_{fu}$ [6,21].

3. Stress limitation and effect of creep rupture on design

Stresses of FRP RC flexural members are limited in a similar way as for conventional steel RC members. When using FRP reinforcement, the major differences arise from the linear behaviour up to failure and the consideration of its lower strength under sustained stresses (creep rupture), previously mentioned. Although the limits in the different codes and guidelines are based on the same principles, their values, as well as procedures and results, may differ from each other.

Concrete compression stresses in EC2 and MC2020 are similarly limited to $0.6f_{ck}$ to avoid longitudinal cracking under the characteristic combination for certain exposure classes. Mention is done about possible effects of non-linear creep of concrete for high stresses under quasi-permanent loads.

For conventional steel RC, codes propose stress limitations under SLS conditions while in ULS the stress is limited by the design strength, based on the yield strength. Similarly, both types of limitation are applied to FRP RC design, although the way in which creep rupture is considered may represent a relevant difference. In the codes analysed in this work the effect of creep rupture is included in SLS design in ACI440.11, while EC2 and MC2020 additionally incorporate it in the ULS calculations. Therefore, the comparison of design among codes would not make sense without including the ULS for bending in EC2 and MC2020.

Stresses under SLS combinations of actions are calculated following the usual assumptions of fully cracked section and linear behaviour of materials:

$$\sigma_f = \frac{\alpha \cdot M \cdot (d - x)}{I_{cr}} \tag{6}$$

where $\alpha = E_f/E_c$ is the ratio between moduli of elasticity of FRP reinforcement and concrete, M is the flexural moment under the relevant combination of actions, d is the effective depth, x is the neutral axis depth and I_{cr} is the moment of inertia of the transformed cracked section.

In EC2, the limitation for SLS reinforcement stresses follows a similar framework as for steel with a limit equal to the design tensile strength, f_{ftd}, under the quasi-permanent combination to avoid excessive crack width and to $0.8f_{ftd}$ under the characteristic combination of actions to avoid failure at SLS.

In MC2020, the stresses under the quasi-permanent combination should not exceed the stress limit for FRP creep rupture, $\sigma_{f,creep,Rd}$.

In the case of ACI440.11, the stress caused by the sustained loads (assimilable to the concept of quasi-permanent loads) should be lower than $f_{fs,sus\ max} = 0.30f_{fu}$.

The inclusion of the creep rupture tensile strength in the ULS calculations in some codes [8,10] may have a relevant impact on the design. Although the basis of design for FRP RC bending members are the same as for steel RC, the linear elastic behaviour up to failure introduces some changes in the conventional procedures. Bending failure may be due either to concrete crushing (compression-controlled) or tensile FRP rupture (tension-controlled), and both types of failures are accepted by existing provisions. Due to their low modulus of elasticity GFRP RC beams will

have large deflections at rupture, mainly for tension-controlled sections [6]. The equations governing both types of failure are slightly different; therefore, for the calculations, it will be necessary to check which is the expected failure mode. Essentially, in compression-controlled sections, the FRP stress at failure will be lower than its design strength. In contrast, for tension-controlled sections, the FRP will attain its design strength, while the concrete will not reach its ultimate strain. A summary of the procedures and equations for the three codes compared in this work can be found in Appendix B. Figure 2 presents a non-dimensional design chart following EC2 or MC2020 procedures in which it is seen a unique curve for concrete failure and different curves for FRP rupture, depending on the reinforcement design strain. The intersection point indicates the change in model of failure. Details about the design procedure for bending FRP RC elements can be found in [24].

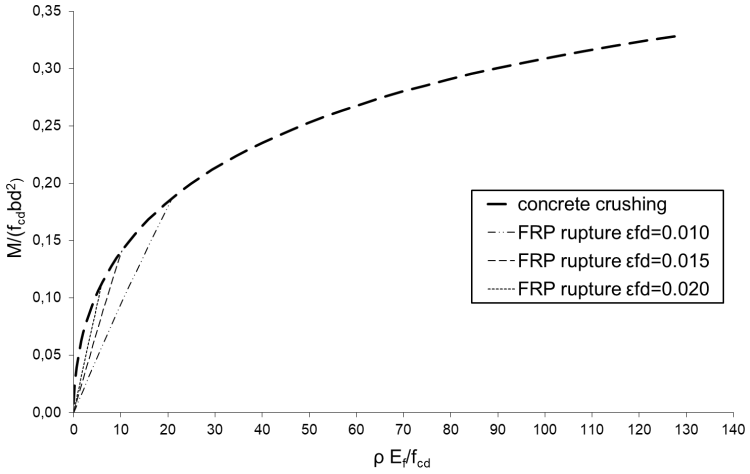

Figure 2. Design chart for flexural capacity of FRP RC members.

4. Crack control

Because of its low tensile strength, concrete usually cracks under the tensile stresses due to bending forces. The main reasons to limit crack width are due to its incidence on the appearance, durability or functionality of the structure. Regarding the FRP reinforcement, most recommendations take into account the non-corrosive properties of FRP and propose a relaxation of usual crack limits in absence of appearance or functionality restrictions (e.g. water tightness).

The approaches for crack control in codes for FRP RC are similar to those for steel RC, with slight modifications to account for the FRP characteristics.

Crack control in the last versions of EC2 and MC2020 is based on the same procedure, although equations may apparently look different when compared. For convenience in the exposition of the conceptual basis, the equations and notation from MC2020 are summarized in the following.

In order to meet the requirements for crack control, the crack width must satisfy the condition:

$$w_{cal} \leq w_{lim} \tag{7}$$

where w_{cal} is the design (or calculated) crack width and w_{lim} is the nominal limit considered at the concrete surface. It is emphasized that due to the highly probabilistic nature of cracking, calculated values are intended for comparison with nominal limits, and the actual measured crack widths can differ from these nominal calculated values [8].

It is considered that the procedures for steel may be applied for FRP reinforcement, provided that the corresponding material properties are used.

The crack width calculations are based on the behaviour of a prismatic RC tensile element with a simplified load-strain law with constant tension-stiffening effect after a horizontal line for the crack formation stage (Figure 3).

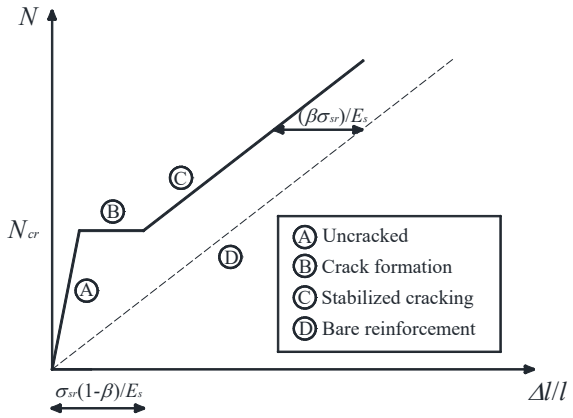

Figure 3. Load-strain model for crack control (adapted from [8]).

The calculated crack width is estimated as the product of the maximum crack spacing, $s_{r,max}$, and the difference of mean strains of FRP reinforcement and concrete (ε_{fm} - ε_{cm}):

$$w_{cal} = k_{1/r} \cdot s_{r,max} \cdot \left(\varepsilon_{fm} - \varepsilon_{cm}\right) \tag{8}$$

$$k_{1/r} = \frac{h - x}{d - x} \tag{9}$$

where $k_{1/r}$ accounts for the increased crack width at the concrete surface due to curvature in bending, being h the total depth of the section, d the effective depth and x the neutral axis depth of the fully cracked section.

The maximum crack spacing can be obtained by:

$$s_{r,max} = \beta_w \left(k_c \cdot c + k_{\phi/\rho} \cdot k_{fl} \cdot k_b \frac{f_{ctm}}{\tau_{bmf}} \frac{\phi}{\rho_{f,ef}}\right) \tag{10}$$

being β_w a factor to obtain maximum crack spacing from mean crack spacing (1.7 for stabilized cracking and 2.0 for crack formation stage); k_c a parameter to consider influence of concrete cover; c is the clear cover; $k_{\phi/\rho}$ quantifies the influence of the mean bond strength τ_{bmf} (assumed as 0.25); k_{fl} accounts for stress distribution before cracking (pure tension, bending); k_b accounts for poor bond conditions (1.2) or good bond conditions (0.9); f_{ctm} is the mean tensile strength of concrete; ϕ is the bar diameter; and $\rho_{f,ef}$ is the effective reinforcement ratio (in a defined effective concrete area in tension surrounding the bars, $A_{c,ef}$). By default, this procedure assumes a bond effect between FRP and concrete similar to that of steel reinforcement, although the equation contains parameters to consider the influence of bond.

The mean strain difference for elements subjected to direct load may be calculated as:

$$\varepsilon_{fm} - \varepsilon_{cm} = \frac{\sigma_f - \beta_{TS} \cdot \sigma_{fr,ef}}{E_f} \geq \frac{\sigma_f}{E_f}(1 - \beta_{TS}) \tag{11}$$

with

$$\sigma_{fr,ef} = \frac{f_{ctm}}{\rho_{f,ef}}\left(1 + \alpha_e \cdot \rho_{f,ef}\right) \tag{12}$$

where σ_f is the reinforcement stress in the cracked section; E_f is the modulus of elasticity of FRP reinforcement; α_e is the modular ratio E_f/E_c; and β_{TS} is 0.6 for crack formation stage and short-term loading in stabilized cracking, and 0.4 for long-term loading in stabilized cracking.

According to EC2, the limiting value of crack width under the quasi-permanent combination is 0.4 mm for appearance requirements. In absence of appearance conditions, fasteners, punctual wheel pressure, lap splice or freeze thaw, this limit may be relaxed to values up to 0.7 mm. The same limitations apply in MC2020.

Control of cracking in ACI440.11 is carried out by limiting the longitudinal reinforcement spacing using a procedure developed in [25] based on modifications of [26]. Instead of obtaining a calculated value of crack width to be compared with a limiting value, the equations have been arranged by introducing a crack width limit of 0.7 mm, to explicitly obtain a maximum allowed value of reinforcement spacing, having at the same time to satisfy a maximum reinforcement stress:

$$s \leq \frac{0.81 \cdot E_f}{f_{fs} \cdot k_b} - 2.5 \cdot c_c \not> 0.65 \frac{E_f}{f_{fs} \cdot k_b} \tag{13}$$

$$f_{fs} \leq \frac{0.36 \cdot E_f}{d_c \cdot k_b \cdot \beta_{cr}} \tag{14}$$

where c_c is the least distance from bar surface to tension face; d_c is the concrete cover to centre of bar; f_{fs} is the tensile stress at service loads; β_{cr} is the ratio of the distance from neutral axis to extreme tensioned fibre to the distance from neutral axis to centroid of reinforcement; and k_b is a bond factor taken as 1.2 for GFRP. In specific situations where a smaller crack width value is judged to be appropriate, the coefficients 0.81 and 0.36 can be adjusted linearly.

5. Deflection control

Excessive deflections of RC flexural members may derive in problems of appearance, integrity of non-structural elements or loss of functionality of the structure or equipment. To avoid the aforementioned problems, deflections are limited generally to a fraction of the member span. Since these effects are independent of the type of reinforcement, the same limits as for steel RC apply for FRP RC members.

Because of the many factors that influence deflections, the actual values can differ significantly from those calculated. Uncertainties in assessing the actual material properties, loading history, construction procedures, assessment of member forces, and environmental conditions may have a strong influence on deflections. In that sense, calculated deflections (as for the case of crack width) should be taken as reference values intended for comparison with specified limits [8,27,28].

The relatively low modulus of elasticity of FRP reinforcement (mainly for GFRP), makes them susceptible to experience large deflections. However, the same basis and subsequent formulation for assessing the flexural deformations of steel RC members applies also for FRP reinforcement as experimentally proven. For short-term deflections, the main aspect to take into account is the change in the modulus of elasticity. Since long-term deformations depend on the sectional area of concrete creeping and shrinking (i.e. the neutral axis depth), a reinforcement with different stiffness may lead to a different ratio between short and long-term deflections (lower if the modulus of elasticity is lower) [29]. In that sense, methods based on general procedures [8,10], where the main properties can be introduced, may be directly applied. On the other hand, simplified methods for steel RC based on multiplicative coefficients may need some adjustment [30-32].

Calculation of deflections for FRP RC members in EC2 follows the general procedure in the main body of the code for steel RC. Deformation of cracked members is obtained as an interpolation of sectional deformations in uncracked and fully cracked states:

$$a = (1 - \zeta) \cdot a_I + \zeta \cdot a_{II} \tag{15}$$

where a is the deformation parameter considered (strain, curvature or rotation; as a simplification, it may also be taken as deflection) and subscripts *I* and *II* account for uncracked and fully cracked states; and ζ is a distribution coefficient (allowing for tension-stiffening effect) given by:

$$\zeta = 1 - \beta_t \left(\frac{\sigma_{fr}}{\sigma_f}\right)^2 \geq 0 \tag{16}$$

with $\zeta = 0$ for uncracked sections; β_t equal to 1.0 for single short-term loading or 0.5 sustained/repeated loading; σ_f is the highest tensile reinforcement stress having occurred; σ_{fr} is the reinforcement stress under the cracking conditions. In case of flexure σ_{fr}/σ_f may be replaced by the ratio of corresponding bending moments M_{cr}/M.

The effective tensile strength of the concrete, $f_{ct,eff}$, may be taken as the mean axial tensile strength, f_{ctm}, or the mean flexural tensile strength, $f_{ct\,fl}$.

Long-term deflections due to creep are calculated using transformed sections through the effective modulus of elasticity of concrete, $E_{c,eff}$:

$$E_{c,eff} = \frac{1.05 E_{cm}}{1+\varphi} \tag{17}$$

where E_{cm} is the secant modulus of elasticity of concrete; and φ is the concrete creep coefficient.

Shrinkage deflections can be calculated from sectional curvatures given by:

$$\left(\frac{1}{r}\right)_{\varepsilon_{cs}} = \varepsilon_{cs} \frac{E_f}{E_{c,eff}} \frac{S_i}{I_i} \tag{18}$$

being ε_{cs} the shrinkage strain; S_i the first moment of the reinforcement about the centroid of the long-term transformed cross-section for the uncracked ($i = I$) or fully cracked ($i = II$) conditions; and I_i the second moment about the centroid of the long-term transformed cross-section for the states *I* and *II*.

For a rigorous calculation, deflections can be assessed from double integration of averaged sectional curvatures along the member. Since the deflection is very sensitive to the curvature of the determinant section, a more simplified procedure consists in the interpolation of member deflections in states *I* and *II*. This simplification is equivalent to use an effective moment of inertia for the flexural element, deduced by introducing curvatures ($(1/r) = M/(E \cdot I)$) in Eq. (15) [9,33,34]:

$$I_{ef} = \frac{I_I \cdot I_{II}}{\zeta \cdot I_I + (1-\zeta) \cdot I_{II}} \tag{19}$$

that replacing ζ from Eq. (16) may be rearranged to [18,35]:

$$I_{ef} = \frac{I_{II}}{1 - \beta_t \cdot \left({}^{M_{cr}}/_{M}\right)^2 \left(1 - {}^{I_{II}}/_{I_I}\right)} \tag{20}$$

Figure 4 shows a typical representation of the sectional moment-curvature behaviour.

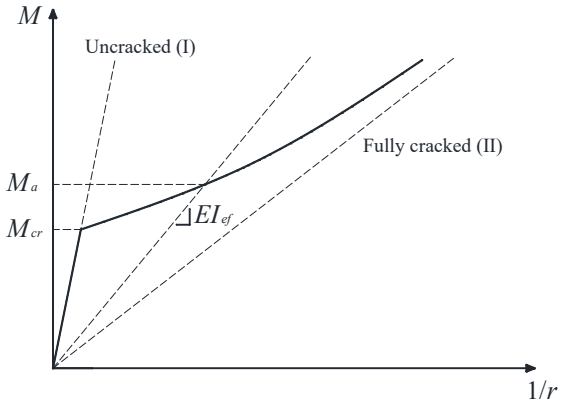

Figure 4. Moment-curvature and I_{ef}.

According to the Eurocodes [36], the total long-term deflection under the quasi-permanent combination is limited to $L/250$, which has been the criterion to deduce the proposed span-to-depth ratios to comply with deflection limitations in EC2.

MC2020 introduces three levels of approximation to calculate deflections due to bending, which are based on the same principles and general methodologies exposed in previous versions of fib Model Code [9,37] and Eurocode 2 [38]. A general method (LoA III) and a simplified method for RC structures (LoA II) are applicable to FRP RC members.

LoA III refers to methodologies based on nonlinear numerical analysis of reinforced and prestressed concrete structures accounting for the most relevant aspects influencing their actual behaviour: cracking, time-dependent properties, load history, construction sequence, deterioration or retrofitting, among others [28,39-50]. MC2020 explicitly includes as an option for a general approach, the procedure already mentioned for EC2 (Figure 4, Eqs. (15-18)) to obtain averaged sectional deformations from interpolation between the uncracked and cracked states and consequent integration along the member [45,47]. In this case, the bending moments can be approximated by linear analysis and subsequent redistribution if needed. It also has been implemented in general models for nonlinear serviceability analysis of beams and frames [51]. Other methodologies for accounting of cracking and tension-stiffening, such as those based on modified constitutive models for concrete or steel, would also be included among the nonlinear procedures [52-55].

The simplified method LoA II is derived from LoA III and is appropriate for RC flexural members either simply supported or continuous with or without side cantilevers, and fixed-end cantilevers. It allows usual sections shapes (rectangular, T, I) and variable reinforcement layout along the member. No explicit integration of curvatures is needed; cracking, tension-stiffening, creep and shrinkage of concrete are considered [8,28].

The instantaneous deflections are calculated interpolating deflections in the uncracked (the gross section may be used) and fully cracked states (with averaged tensile and compressive reinforcement ratios along the member) by using Eq. (15) and adopting a secant modulus of elasticity of concrete $E_c = 0.9E_{ci}$. The distribution factor in Eq. (16) is modified to:

$$\zeta = k_e \left[1 - \beta \left(\frac{M_{cr}}{M_a}\right)^2\right] \tag{21}$$

where M_{cr} is calculated with f_{ctm}; M_a is obtained from the characteristic combination; and k_e accounts for the uncracked parts of the beam on the global member stiffness, an effect that may be relevant for low reinforcement ratios and high concrete strength (i.e. relatively high ratio M_{cr}/M_a). For simply supported and continuous beams: $k_e = 1$ for $M_{cr}/M_a \leq 0.5$, and

$k_e = 2 \cdot (1 - M_{cr}/M_a)$ for $0.5 < \frac{M_{cr}}{M_a} \leq 1$; while for cantilevers: $k_e = 1 - (M_{cr}/M_a)^2$ for $0.5 < \frac{M_{cr}}{M_a} \leq 1$.

The time-dependent deflection is computed as the sum of creep and shrinkage deflections. For cracked sections, creep deflection will be assessed by applying a multiplicative factor to the previously calculated instantaneous deflection due to quasi-permanent loads. The factor is deduced considering a cracked section where the effect of creep causes a redistribution of compressive concrete stresses, while the stress in the tensile reinforcement is assumed constant, which is very close to experimental behaviour [45,56,57]. A detailed deduction can be found in [28]. Equilibrium and compatibility equations lead to:

$$a_\varphi = a_{i,qp}(t_0)\frac{x_0}{d}\frac{0.8 \cdot k_t \cdot \varphi}{1+12 \cdot \alpha \cdot \rho'_m} \tag{22}$$

where $a_{i,qp}$ is the instantaneous deflection due to quasi-permanent load; x_0 is the instantaneous neutral axis depth computed with the averaged tensile ($\rho_m = \Sigma(\rho_i \cdot l_i)/\Sigma l_i$) and compressive ($\rho'_m = \Sigma(\rho'_i \cdot l_i)/\Sigma l_i$)) reinforcement ratios along the member; φ is the creep coefficient; α is the modular ratio E_f/E_c; and $k_t = 0.3 + 100\rho_m \leq 1$ is a correction factor to account for the uncracked parts of the beam calibrated through LoA III method [44].

The shrinkage deflection is calculated by integration of curvatures due to shrinkage, accounting for free shrinkage strain, effective depth, element length and boundary conditions. For a cracked member:

$$a_{cs} = k_s k_t \psi_{cs} \frac{l^2}{8} \tag{23}$$

being ψ_{cs} a reference curvature given by:

$$\psi_{cs} = \frac{\varepsilon_{cs}}{d}\frac{1}{1+12\alpha\rho'_m} \tag{24}$$

where ε_{cs} is the shrinkage strain and k_s an integration factor that may be taken as 1 for simply supported beams, 0.7 for end spans of continuous beams and 0.85 for interior spans.

MC2020 suggests limiting total deflections to $L/250$ under the quasi-permanent combination for appearance requirements and general utility of the structure.

The ACI 440.11 code for GFRP RC structures follows the framework of ACI 318-19 for steel RC [58]. Current equations for deflection calculation in ACI formulate an effective moment of inertia [18], I_e, equivalent to a weighted average of flexibility based on the concept indicated in Eqs. (19) and (20) [32,59].

The effective moment of inertia to calculate immediate deflections in GFRP RC cracked members is obtained from:

$$I_{ef} = \frac{I_{II}}{1-\gamma\left({}^{M_{r,cr}}/_{M}\right)^2\left(1-{}^{I_{cr}}/_{I_g}\right)} \qquad \text{for } M_a \geq M_{r,cr} \tag{25}$$

where $M_{r,cr}$ is a reduced cracking moment to account for restraints and reduced tensile strength that is set to $0.8M_{cr}$ for GFRP members (instead of $0.67M_{cr}$ used for steel RC) [58,60]; M_{cr} is calculated using the gross moment of inertia, I_g, and the modulus of rupture of concrete, f_r; and γ accounts for the variation of stiffness over the member length due to the bending moment diagram [60], whose value for uniformly distributed load is given by:

$$\gamma = 1.72 - 0.72\left(\frac{0.8M_{cr}}{M_a}\right) \tag{26}$$

It is worth noting that the use of the factor $\beta = 0.5$, for sustained or repeated loading in EC2 and Model Code equations, causing a shift in the deformation response, would be equivalent to the effect of a reduced cracking moment of $\sqrt{0.5}M_{cr} = 0.71M_{cr}$ (for $M \geq M_{cr}$), in between those used in ACI for steel and FRP reinforcement [32].

For slabs and continuous beams, the effective moment of inertia may be taken as a weighted average of the critical positive and negative moment sections.

The time-dependent deflections are assessed by multiplying the short-term deflections due to sustained loads with a reduced factor $\lambda_\Delta = 0.6\xi$, where ξ is taken from ACI 318-19 for steel RC [58]. The method is practical and easy to use in design, although it does not explicitly consider the moduli of elasticity, sectional stiffness, creep coefficient or shrinkage strain, which may present different values and have relevant influence on the time-dependent-to-immediate deflection ratios [29,30,61].

In ACI440.11, the immediate deflection due to live load of floors not supporting elements likely to be damaged is limited to $L/360$, while the increment of deflection after installation of the non-structural elements is limited to $L/240$. When the floor supports elements likely to be damaged, the increment of deflections after installing those elements is $L/480$.

6. Comparison – design example

This section presents an illustrative example of design of a simply supported reinforced concrete beam of a building for service and administrative uses subjected to a marine environment, with the aim of comparing the procedures of the different codes when designing the longitudinal GFRP reinforcement to accomplish the different serviceability limit states.

The geometry of the beam, with a rectangular cross-section of 300 × 470 mm and a span length of 4.5 m, is shown in Figure 5. The effective depth is taken as 415 mm, accomplishing the different cover requirements for all considered codes. The reinforcement rebars are distributed in one layer.

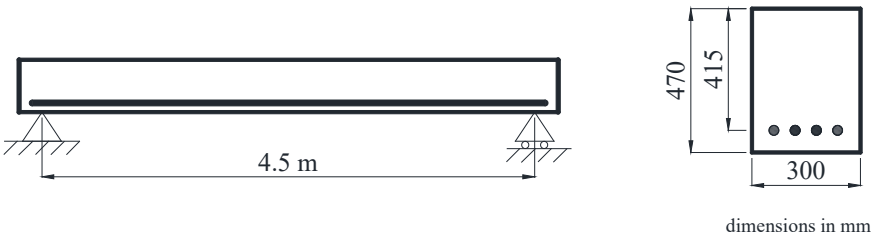

Figure 5. Geometry of the studied beam.

The loads acting on the structure consist of a uniformly distributed permanent (dead) load of g = 16 kN/m (including self-weight), and a variable load (live) q = 10 kN/m, resulting in a characteristic (service) load $g + q$ = 26 kN/m. The combination factor for quasi-permanent (sustained) loads is $\psi_2 = 0.3$. Table 1 shows the maximum bending moment at midspan for the different load combinations that should be considered for design at Ultimate Limit State (ULS) and Serviceability Limit State (SLS). It is assumed that a pre-cracking load corresponding to the characteristic load is applied at 28 days to globally represent effects on cracking level of construction loads.

Table 1. Maximum bending moment at midspan for the different load combinations.

Combination	ULS	SLS characteristic (service)	SLS quasi-permanent (sustained)
EC2/MC2020	M_{Ed} = 92.6 kN·m	M_k = 65.8 kN·m	M_{qp} = 48.1 kN·m
ACI440.11	M_u = 89.1 kN·m	M_s = 65.8 kN·m	M_{sus} = 48.1 kN·m

Material mechanical properties are summarized in Tables 2 and 3. The characteristic concrete compressive strength is f_{ck} = 35 N/mm^2, assuming a weighted creep coefficient to take into account loading history of φ = 1.60 [8,52] and a shrinkage strain of ε_{cs} = 0.000450. For the sake of simplicity, the specified concrete strength, f_c', in ACI has been assumed equal to the characteristic strength, f_{ck}, in EC2 and MC2020. Concrete material properties have been calculated according to the different codes (see Appendix A). As can be seen, there are some differences in the nominal values of the moduli of elasticity, which is due to the definition of each code (secant, tangent). As for the tensile strengths, EC2 uses the mean axial tensile strength, f_{ctm}, for crack control calculations, while for deflection control both mean axial tensile strength and flexural strength, $f_{ctm,fl}$, can be considered according to the designer's criteria. In this example, both values were used for comparative purposes. For the case of MC2020, f_{ctm} is used for both crack and deflection control. Definitions of f_{ctm} from these codes are just slightly different. Finally, the tensile strength value according to ACI (modulus of rupture) is in that case similar to the flexural tensile strength according to EC2.

The GFRP characteristic tensile strength is f_{ftk0} = 1000 N/mm^2 and the modulus of elasticity is E_f = 60000 N/mm^2. The value of characteristic tensile f_{ftk0} strength was assumed equal to the guaranteed tensile strength in ACI, f_{fu}^*. The long-term strength (100 years) is assumed to be provided by the manufacturer from creep rupture tests according to ISO 10406-1 and is taken as $f_{ftk,100a}$ = 480 N/mm^2. If the manufacturer has not performed the tests to characterize the long-term strength, then $f_{ftk,100a}$ can be conservatively evaluated using Eq. (2). Depending on the environmental conditions (indoor or outdoor), this value is obtained as 245 N/mm^2 or 196 N/mm^2, respectively. As observed, the absence of tests may lead to significantly lower values.

Tables 4 to 6 show the minimum area of reinforcement needed to accomplish the requirements for the aforementioned design aspects in relation to the different provisions under study (EC2, MC2020 and ACI440.11). In addition, the disposed number of rebars assuming a diameter of 16 mm, is given in each Table.

In this example, deflections have been calculated by means of the common simplified procedure of interpolation of member deflections in uncracked and fully cracked states. The use of f_{ctm} or $f_{ctm,fl}$ for calculating M_{cr} has been traditionally based on the consideration of the existence or not of residual tensile stresses that may cause a reduction of cracking moment [38]. According to EC2 (Table 4), if the long-term strength of the FRP rebars ($f_{ftk,100a}$) is obtained from tests, the more restrictive criteria is deflection control when using f_{ctm} to obtain the cracking moment (755 mm^2), while using $f_{ctm,fl}$ would require a slightly lower reinforcement area (711 mm^2). This way, if $f_{ctm,fl}$ is used the more restrictive value would be that given by the effect of creep rupture of FRP rebars on the flexural capacity (730 mm^2). In any case, the obtained results are not very different and lead to the same number of FRP rebars (4∅16). It is worth noting that the absence of creep rupture tests, and therefore the assessment of the long-term strength from Eq. (2) with $f_{fk,100a}$ = 245 MPa, would have given the largest FRP area as a requirement for flexural capacity, with a value of 1425 mm^2 (88.7% higher). Consequently, when applying the EC2 provisions the importance of characterizing the long-term strength through experiments should be highlighted.

Table 2. Material properties according to EC2 and MC2020.

	GFRP bars			*Concrete*		
	f_{ftk0} (N/mm^2)	$f_{ftk,100a}$ (N/mm^2) (indoor)	f_{ftd} [3] (N/mm^2)	f_{ctm} (N/mm^2)	$f_{ctm,fl}$ (N/mm^2)	E_c (N/mm^2)
EC2	1000	480[1] 245[2]	320 163	3.21	3.63	33282[4]
MC2020	1000	480[1]	711	3.30	-	34962[5]

(1) Data from tests developed by suppliers.
(2) Indoor value from EC2 (Annex R) in absence of tests (see Sect. 2).
(3) See Sect. 2.
(4) Secant modulus.
(5) Tangent modulus.

Table 3. Material properties according to ACI440.11

	GFRP bars			*Concrete*	
	f_{fu}^* (N/mm^2)	f_{fu} (N/mm^2)	$f_{fs,sus\ max}$ (N/mm^2)	f_r (N/mm^2)	E_c (N/mm^2)
ACI440	1000	850	255	3.67	27806[1]

(1) Secant modulus.

SLS of deflection also controls design according to MC2020 (Table 5). Both LoAII and LoAIII were considered. For the LoAIII approach, the option indicated in MC2020 based on integration along the member of averaged sectional curvatures between the uncracked and cracked states and consequent has been used here. Its application to the example gives a minimum longitudinal reinforcement area of 665 mm^2 for LoAII, while a similar slightly lower value of 648 mm^2 is obtained from LoAIII. In comparison with the EC2 procedure, it is seen that the effect of creep rupture on flexural capacity provisions is not as relevant in this case. Using the same value of the long-term strength obtained from tests (i.e. 480 MPa) the design tensile strength, f_{fd}, according to Eq. (3) would be 711 MPa, that represents a noticeable increase over the value f_{ftd} = 320 MPa applied for EC2. Consequently, the area needed for this requirement is 330 mm^2, which is 43.8 % of 730 mm^2 for EC2.

According to ACI440.11 (Table 6), the total area of reinforcement required for SLS deflections is 763 mm^2, which in this case is very close to the value obtained from EC2 and not very different to those from MC2020. The case of floors not supporting elements likely to be damaged has been considered, and as exposed in Sect. 5, the immediate deflection due to live load has been limited to L/360, and the increment of deflection after installation of the non-structural elements to L/240, being the last one the most restrictive for the required area of reinforcement.

In relation to the cracking verification, the default value in EC2 for maximum crack width is 0.4 mm, due to appearance conditions. In absence of these conditions the value can be increased up to 0.7, which for comparison purposes has been used in this section for the calculations since it is the default value in ACI440.11 (although the code also allows more restricted values according to the designer's criteria). As indicated in the table footnotes, for crack width calculations a diameter must be previously assumed, in that case 16 mm. Based on these assumptions, the requirements for crack control from the three codes have resulted in lower reinforcement areas than those previously discussed. When cracking is verified following EC2 and MC2020, the bottom reinforcement is located in good casting conditions and k_b = 0.9. The required area for both EC2 and MC2020 is the same (590 mm^2), because both formulations are similar. When designing according to ACI440.11, crack control requires a higher amount of longitudinal reinforcement (744 mm^2) compared to EC2 and MC2020, although it has not been the conditioning criteria.

In case of limiting the crack width to 0.4 mm, EC2 and MC2020 provisions would have resulted in 857 mm^2 that corresponds to 5∅16. For this limitation, ACI440 provisions would have led to 1076 mm^2, corresponding to 6∅16, which could not be allocated in one layer. Thus, a rebar diameter of 19 mm would be more convenient, requiring in this case a reinforcement area of 1115 mm^2 (4∅19).

For the FRP stress limitation condition related to creep rupture under SLS, and according to EC2, the verification of stresses for the characteristic combination of actions is more restrictive than that of the quasi-permanent combination of actions. In the first case, the stresses in the reinforcement for the characteristic combination are compared to 80% of the design value of the long-term strength, and in the verification of the quasi-permanent stresses, the comparison is with the design value of the long-term strength. In the last case, the effective properties of the cross-section have been used. As indicated in Table 4, the required area for SLS stress limitation in case of using the long-term strength from tests in EC2 would be 428 mm^2. In absence of tests, use of long-term strength from Eq. (2) would require 850 mm^2.

MC2020 only considers the verification of stresses under sustained conditions. Therefore, the quasi-permanent combinations of actions is used. The sustained stress should be lower than the design value of the stress limit for creep rupture which in that case is equal to the long-term strength of the FRP affected by a factor of 0.85 as seen in Eq. (4). The application of these combinations and limitations globally leads to a required area is 298 mm^2 (70% of that in EC2).

As for ACI440.11, the verification of creep rupture through the limitation of stresses is only carried out under SLS. Unlike EC2 and MC2020, the code does not mention the option to use values obtained from tests. For that verification, the stress is calculated for the sustained loading combination and the limit is fixed to 0.30f_{fu}. This leads to a required area of 474 mm^2.

Anyway, for the case of this example, the requirement of stresses under SLS would not be the governing factor for any of the three codes.

Table 4. GFRP reinforcement areas in mm^2 needed to comply with EC2 provisions

EC2	Cracking[1]	Deflection		FRP stresses (SLS)		FRP stresses (ULS) Flexural capacity
		f_{ctm}	$f_{ctm,fl}$	quasi-perm.	charact.	
Strictly required (mm^2)	590[2]	**755**	711	252	428	730[3]
Disposed	3∅16 (603)	4∅16 (804)	4∅16 (804)	2∅16 (402)	3∅16 (402)	4∅16 (804)

(1) Crack width limit of 0.7 mm is assumed, in absence of appearance conditions. A diameter must be assumed for crack control calculations, being in that case ∅16.

(2) Minimum required area which does not correspond to an integer number of bars of ∅16.

(3) Tension-controlled failure (FRP rupture).

Table 5. GFRP reinforcement areas in mm^2 needed to comply with MC2020 provisions

MC2020	Cracking[1]	Deflection		FRP stresses (SLS)	FRP stresses (ULS) Flexural capacity
		LoAIII	LoAII		
Strictly required (mm^2)	590[2]	648	**665**	298	330[3]
Disposed	3∅16 (603)	4∅16 (804)	4∅16 (804)	2∅16 (402)	2∅16 (402)

(1) The cracking model in MC2020 is similar to that in EC2. The same values are obtained, and the same comments apply.

(2) Minimum required area which does not correspond to an integer number of bars of ∅16.

(3) Tension-controlled failure (FRP rupture).

Table 6. GFRP reinforcement areas in mm^2 needed to comply with ACI440 provisions

ACI440.11	Cracking[1]	Deflection		FRP stresses (SLS)	FRP stresses (ULS) Flexural capacity
		Δ_{inc}	$\Delta_{i,L}$		
Strictly required (mm^2)	744[2]	702	**763**	474	495[3]
Disposed	4∅16 (603)	4∅16 (804)	4∅16 (804)	3∅16 (603)	3∅16 (603)

(1) Crack width limit of 0.7 mm is assumed, as default value in the code, in absence of additional requirements. A diameter must be assumed for crack control calculations, being in that case ∅16

(2) Minimum required area which does not correspond to an integer number of bars of ∅16.

(3) Tension-controlled failure (FRP rupture).

Table 7 summarizes the required reinforcement area, the number of rebars considering a 16 mm diameter, and the limiting condition for design for the three codes. It is seen that SLS deflection governs in all cases if in EC2 the long-term strength is characterized through tests and f_{ctm} is used for deflection calculations. In case of using $f_{ctm,fl}$ for deflections in EC2, creep rupture for flexural capacity would govern for this code. Although there are some slight differences among codes, in all cases 4∅16 are needed to globally comply with every requirement. When the long-term strength due to creep rupture in EC2 is not obtained from tests, but assessed through Eq. (2), the reinforcement area would increase up to 1425 mm^2, to comply with the requirements of flexural capacity.

Table 7. Required GFRP reinforcement areas in mm^2 needed to comply with all provisions

FRP area (mm^2)	EC2		MC2020	ACI440.11
Strictly required	755(1)	730(2)	665	763
Disposed	4∅16	4∅16	4∅16	4∅16
Condition	Deflection	Flex. capacity	Deflection	Deflection

(1) Long-term strength characterized through tests and f_{ctm} for deflection control.

(2) Long-term strength characterized through tests and $f_{ctm,fl}$ for deflection control.

The final results in terms of number of rebars required by the different codes in this example are the same and mainly due to deflection control. However, when comparing the different limit states analysed it is seen that there might be larger differences in the verification of cracking and stresses. For the case of stresses the calculation models do not provide significant differences and the divergences are mainly due to the combination of actions and prescribed limits. For the case of cracking, some differences may arise from the calculation models (EC2 and MC2020 versus ACI) as well as from the limitations inherent to each model. It is shown that limiting crack width to 0.4 mm instead of 0.7 mm may cause a significant increment of reinforcement area.

Moreover, it is seen that the value and provisions to account for the long-term design strength due to creep rupture may lead to significant variations in the required reinforcement area. Obtention of this strength through tests, mainly for EC2, seems to be of major importance since the proposed equation may result in very conservative values. Consideration of creep rupture only in SLS or also in ULS may also have relevant incidence. In that context, a more in-depth study on reliability, based on experimental data from commercially available rebars, would be needed to help harmonize the treatment of creep rupture across different design codes.

Finally, it should be emphasized that this is only an illustrative example with the objective to allow comparison and discussion of the main requirements in FRP RC flexural design. These results and conclusions should not be taken as broadly representative, given the number of variables involved in the flexural design of FRP RC and the high variability of properties that may be found among the available products. In that sense, a wide parametric study would be necessary to arrive at more general conclusions.

7. Conclusions

A comparative analysis of existing standards (EC2, MC2020 and ACI440.11) for the design of GFRP RC flexural members has been included in this paper, focusing on the main aspects and provisions for serviceability limit state (SLS). These three standards were selected due to their

relevance at international level. From the performed study the following conclusions can be drawn:

- In general, the design of FRP RC flexural elements follows principles similar to those of steel RC elements, but there are some particularities derived from the linear-elastic behaviour and from the possible creep rupture under sustained loads.
- Stress limitations are applied in all reviewed codes, but with varying allowable stress values. ACI440.11 only addresses creep rupture effects at the serviceability level, while EC2 and MC2020 additionally incorporate it in the ULS calculations.
- The models for crack control are the same in EC2 and MC2020, but different from ACI. For all studied standards, the crack width might be relaxed to values up to 0.7 mm, in the absence of more restrictive conditions such as appearance or water tightness.
- The simplified procedures for deflection calculation of the three codes are based on averaged curvatures leading to an effective moment of inertia in the case of ACI440.11 and allow considering the influence of the uncracked parts of the member. While EC2 and LoA II of MC2020 interpolate between uncracked and fully cracked states, incorporating effects like tension-stiffening, creep, and shrinkage, ACI 440.11 uses a multiplicative factor for long-term deflections.
- The inclusion of creep rupture effects in the ULS verification besides SLS has relevant consequences in the particular case of EC2. In that sense, it is of major importance to assess the long-term strength of the reinforcement through tests, since the proposed equation may lead to very conservative results.
- For the example presented in this paper, SLS deflection governs in all cases. However, for EC2, creep rupture for flexural capacity would govern if $f_{ctm,fl}$ is used to calculate the cracking moment when checking deflections. For cracking, it is seen that limiting crack width to 0.4 mm instead of 0.7 mm may cause a significant increment of reinforcement area. For SLS stresses the divergences are mainly due to the combination of actions and prescribed limits.
- Given the numerous variables involved, a wide parametric analysis is required to reach generalized conclusions.

Acknowledgements

This article is dedicated to Professor Antonio Marí, with whom we have had the privilege to collaborate over a long time in the field of serviceability behaviour of concrete structures. His extensive knowledge, commitment to excellence and leadership have been a reference and source of inspiration for us. We also extend this dedication to Professor Hugo Corres, for his valuable contributions to the field of structural concrete.

We would also like to acknowledge the financial support provided by projects CPP2022-009555 and PCI2023-143361 funded by MICIU/AEI/10.13039/501100011033, European Union-NextGenerationEU/PRTR and by ERDF/EU.

Appendix A: Concrete mechanical properties in codes

A1. EC2 (2023)

$$f_{ctm} = 0.3 \cdot f_{ck}{}^{2/3} \quad \text{for } f_{ck} \leq 50 \text{ MPa} \tag{A1}$$

$$f_{ctm,fl} = \max\left\{\left(1.6 - {}^{h}/_{1000}\right) f_{ctm};\ f_{ctm}\right\} \tag{A2}$$

$$f_{cd} = \eta_{cc} k_{tc} {}^{f_{ck}}/_{\gamma_C} \tag{A3}$$

with γ_C = 1,5 for persistent and transient situations, and

$$\eta_{cc} = \left({}^{40}/_{f_{ck}}\right)^{1/3} \leq 1.0 \tag{A4}$$

$$k_{tc} = 1.0 \quad \text{for } t_{ref} \leq 28 \text{ days} \tag{A5}$$

$$E_{cm} = k_E (f_{ck} + 8)^{1/3} \tag{A6}$$

with $k_E = 9500$ for quartzite aggregates.

$$E_{c,eff} = {}^{1.05 \cdot E_{cm}}\Big/_{\left(1 + \varphi(t, t_0)\right)} \tag{A7}$$

where f_{ck} = characteristic compressive strength; f_{ctm} = mean axial tensile strength; $f_{ctm,fl}$ = mean flexural tensile strength; h = total depth of the section; f_{cd} = design compressive strength; γ_C = partial factor for concrete; E_{cm} = secant modulus of elasticity of concrete; $E_{c,eff}$ = effective modulus of elasticity accounting for creep deformations; $\varphi(t, t_0)$ = creep coefficient at the age of loading.

A2. MC2020

$$f_{ctm} = 1.8 \cdot \ln(f_{ck}) - 3{,}1 \tag{A8}$$

$$f_{ctm,fl} = f_{ctm}{}^{(1 + 0.06 \cdot h^{0,7})}\Big/_{0{,}06 \cdot h^{0,7}} \tag{A9}$$

$$f_{cd} = \alpha_{cc} \cdot \eta_{fc} \cdot {}^{f_{ck}}/_{\gamma_C} \tag{A10}$$

with γ_C = 1.5 for persistent and transient situations, α_{cc}=1.0 for new structures and

$$\eta_{fc} = \left({}^{40}/_{f_{ck}}\right)^{1/3} \leq 1.0 \tag{A11}$$

$$E_{ci} = E_{c0} \cdot \alpha_E \left({}^{(f_{ck} + 8)}/_{10}\right)^{1/3} \tag{A12}$$

with $\alpha_E = 1.0$ for quartzite aggregates and E_{c0} = 21500.

$$E_{c,ef} = {E_{ci}}/{\left(1 + \varphi(t, t_0)\right)} \quad \text{(A13)}$$

where E_{ci} = tangent modulus of elasticity and the rest of symbols are the same as those defined for EC2 (2023).

A3. ACI 440.11-22

$$f_r = 0.62 \cdot f_c' \quad \text{(A14)}$$

$$E_c = 4730\sqrt{f_c'} \quad \text{(A15)}$$

where f_r = modulus of rupture (flexural tensile strength); f_c' = specified compressive strength; E_c = secant modulus of elasticity.

Appendix B: Summary of procedures for the ULS of bending with FRP reinforcement

B1. Types of failure

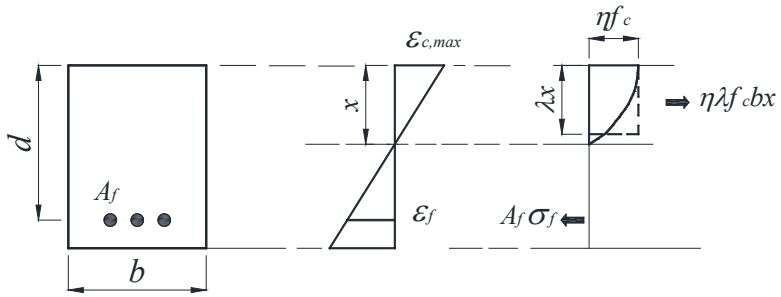

Figure B1. Sectional strains, stresses and parameters.

There are two possible modes of failure: a) concrete failure (compression-controlled) and b) FRP failure (tension-controlled). The balanced condition can be defined as that in which failure is attained simultaneously for both materials:

$\varepsilon_{c,max} = \varepsilon_{cu} \qquad \varepsilon_f = \varepsilon_{fd} = f_{fd}/E_f$

where ε_c is the concrete strain; ε_{cu} is the ultimate compressive concrete strain; ε_f is the reinforcement strain; f_{fd} is the FRP design tensile strength already defined for each code in Sect. 2 (named f_{fu} in ACI440.11); and E_f is the modulus of elasticity of FRP.

The balanced reinforcement ratio, ρ_{fb}, can be obtained from equilibrium and compatibility equations:

$$\rho_{fb} = \eta \cdot \lambda \frac{f_{cd}}{f_{fd}} \frac{E_f \cdot \varepsilon_{cu}}{E_f \cdot \varepsilon_{cu} + f_{fd}} \tag{B1}$$

and therefore

$\rho_f > \rho_{fb}$ concrete failure; $\rho_f \leq \rho_{fb}$ FRP failure

where λ, η are parameters defining the equivalent rectangular stress block of concrete, and f_{cd} is the concrete design strength for each code.

B2. Eurocode 2 (2023)/fib Model Code 2020

The design bending moment M_{Ed} must be lower than the moment capacity M_{Rd}

$M_{Ed} \leq M_{Rd}$

where, for a combination case of simple bending with one variable action

$$M_{Ed} = 1.5 \cdot M_q + 1.35 \cdot M_g \tag{B2}$$

being M_q and M_g the bending moments due to variable loads and permanent loads, respectively.

The concrete design strength is $f_{cd} = f_{ck}/\gamma_c$, where f_{ck} is the characteristic design strength, while the material partial factor for concrete is $\gamma_c = 1.5$.

Although theoretically the parameters of the rectangular stress block depend on the maximum concrete strain attained, assumption of $\eta = 1$, $\lambda = 0.8$ for both concrete and tension failure leads to simplification in calculations with accurate enough values.

B2.1. Compression-controlled failure

$\rho_f > \rho_{fb}$; $\varepsilon_{c,max} = \varepsilon_{cu} = 0.0035$; $\varepsilon_f = \sigma_f / E_f < \varepsilon_{fd}$

from equilibrium of forces and compatibility of deformations:

$$\sigma_f = \left(\sqrt{\frac{\left(E_f \cdot \varepsilon_{cu}\right)^2}{4} + \frac{0.8 \cdot f_{cd}}{\rho_f} E_f \cdot \varepsilon_{cu}} - 0.5 \cdot E_f \cdot \varepsilon_{cu} \right) \leq f_{fd} \tag{B3}$$

and the moment capacity is:

$$M_{Rd} = \rho_f \cdot \sigma_f \left(1 - 0.5 \frac{\rho_f \cdot \sigma_f}{f_{cd}}\right) b \cdot d^2 \tag{B4}$$

where σ_f is the actual reinforcement stress.

B2.2. Tension-controlled failure

$\rho_f \leq \rho_{fb}$ $\quad \varepsilon_{c,max} < \varepsilon_{cu} = 0.0035$ $\quad \varepsilon_f = \sigma_f / E_f < \varepsilon_{fd} = f_{fd} / E_f$

the moment capacity is:

$$M_{Rd} = \rho_f \cdot f_{fd} \left(1 - 0.5 \frac{\rho_f \cdot f_{fd}}{f_{cd}}\right) b \cdot d^2 \tag{B5}$$

B3. ACI440.11-22

The factored bending moment M_u must be lower than the design flexural strength, defined as the nominal flexural strength, M_n, multiplied by a strength reduction factor ϕ.

$M_u \leq \phi \cdot M_n$

where

$$M_u = 1.6 \cdot M_q + 1.2 \cdot M_g \tag{B6}$$

No material partial factors are used; f_{cd} in Figure B.1 must be the specified concrete strength f'_c.

The strength reduction factor depends on the FRP reinforcement strain, with values of 0.65 for a compression-controlled section and 0.55 for a tension-controlled section. A linear transition zone between both values is adopted in the range $0.8\varepsilon_{tu} \div \varepsilon_{tu}$ ($\varepsilon_{tu} = f_{fu}/E_f$), equivalent to $1.4\rho_{fb} \div \rho_{fb}$, which leads to:

$$\phi = \begin{cases} 0.55 & \rho_{fb} \\ 0.30 + 0.25\, {}^{\rho_f}/_{\rho_{fb}} & \rho_{fb} < \rho_f < \rho_{fb} \\ 0.65 & \rho_f \leq 1.4\rho_{fb} \end{cases} \tag{B7}$$

B3.1. Compression-controlled failure and transition zone

The same conditions and equations indicated in EC2/MC2020 for compression-controlled failure apply, taking into account that $\varepsilon_{cu} = 0.003$; f_{fd} is called f_{fu} in the code; and ε_{fd} is called ε_{fu}.

Parameters η and λ of the concrete rectangular stress block, called α_1 and β_1 in the code adopt the following values:

$$\eta = 0.85$$

$$\lambda = \begin{cases} 0.85 & 21 \le f_c' \le 28 \\ 0.85 - 0.05\,(f_c' - 28)/7 & 28 < f_c' \le 55 \\ 0.65 & f_c' \ge 55 \end{cases} \quad \text{(B8)}$$

The calculated M_n (M_{Rd} in previous equations) must be multiplied by the corresponding strength reduction factor ϕ.

B3.2. Tension-controlled failure

The code indicates that the defined coefficients for the concrete rectangular stress block do not apply in this case. The code proposes a simplified and conservative lower bound for M_n based on assuming a neutral axis depth corresponding to the balanced condition, x_b. This way:

$$x_b = \frac{\varepsilon_{cu}}{\varepsilon_{cu} + \varepsilon_{fu}} d \quad \text{(B9)}$$

$$M_n = A_f \cdot f_{fd}(d - \beta_1 \cdot x_b) \quad \text{(B10)}$$

References

[1] L.C. Bank, Composites for Construction: Structural Design with FRP Materials, Wiley, 2007.

[2] fib T.G. 9.3, Bulletin 40. FRP reinforcement in RC structures, Lausanne, Switzerland, 2007.

[3] ACI Committee 440, Guide for the Design and Construction of Structural Concrete Reinforced with Fiber Reinforced Polymer (FRP Bars) (ACI440.1R-15), American Concrete Institute, Farmington Hills, Michigan, USA, 2015.

[4] JSCE, Application of Continuous Fiber Reinforcing Materials to Concrete Structures, *Concrete Library*, No. 72, 1992, published in Japanese.

[5] K. Pilakoutas, M. Guadagnini, K. Neocleous, L. Taerwe, Design guidelines for FRP reinforced concrete structures, in: Proceedings of the 3rd Internatinal Conference Advanced Composites in Construction (ACIC2019), Bath, 2007.

[6] ACI Committee 440, Building Code Requirements for Structural Concrete Reinforced with Glass Fiber-Reinforced Polymer (GFRP) Bars (ACI440.11-22), American Concrete Institute, Farmington Hills, Michigan, USA, 2022.

[7] ACI Committee 440, Guide for the Design and Construction of Structural Concrete Reinforced with FRP Bars, (ACI440.1R-06), American Concrete Institute, Farmington Hills, Michigan, USA, 2006.

[8] fib, fib Model Code for Concrete Structures 2020 v1.2, International Federation for Structural Concrete, Lausanne, Switzerland, 2024.

[9] fib, fib Model Code for Concrete Structures 2010, International Federation for Structural Concrete, Lausanne, Switzerland, 2013.

[10] CEN, Eurocode 2: Design of concrete structures — Part 1-1: General rules — Rules for buildings, bridges and civil engineering structures (EN 1992-1-1:2023), European Committee for Standardization, Brussels, Belgium, 2023.

[11] CNR, Guide for the design and Construction of Concrete Structures Reinforced with Fiber-Reinforced Polymer Bars (CNR-DT 203/2006), Italian National Research Council, Italy, 2007.

[12] CSA, Design and construction of building components with fibre-reinforced polymers (CAN/CSA-S806-12 R17), Canadian Standards Association, Mississauga, Ontario, Canada, 2012.
[13] CSA, Canadian Highway Bridge Design Code (CSA-S6:19), Canadian Standards Association, Mississauga, Ontario, Canada, 2019.
[14] AFGC, Utilisation d'armatures composites (à fibres longues et à matrice orga-nique) pour le béton armé, Association Française de Génie Civil, France, 2021.
[15] JSCE, Recommendation for Design and Construction of Concrete Structures Using Continuous Fiber Reinforcing Materials, Concrete Engineering Series 23, Japan Society of Civil Engineers, Japan, 1997.
[16] A. Nanni, Flexural behaviour and design of RC members using FRP reinforcement, ASCE Journal of Structural Engineering 119 (11) (1993) 3344-59. https://doi.org/10.1061/(ASCE)0733-9445(1993)119:11(3344).
[17] S. Matthys, L. Taerwe, Concrete slabs reinforced with FRP grids. I: One-way bending, ASCE Journal of Composites for Construction 4 (3) (2000) 145-153. https://doi.org/10.1061/(ASCE)1090-0268(2000)4:3(145).
[18] P. Bischoff, Revaluation of deflection prediction for concrete beams reinforced with steel and fiber reinforced polymer bars, ASCE Journal of Structural Engineering 131 (5) (2005) 752-76. https://doi.org/10.1061/(ASCE)0733-9445(2005)131:5(752).
[19] C. Barris, L. Torres, M. Baena, K. Pilakoutas, M. Guadagnini, Serviceability limit state of FRP RC beams, Advances in Structural Engineering 15 (4) (2012) 653-63. https://doi.org/10.1260/1369-4332.15.4.653.
[20] C. Barris, L. Torres, C. Miàs, I. Vilanova, Design of FRP reinforced concrete beams for serviceability requirements. Journal of Civil Engineering and Management 18 (6) (2012) 843 - 857. https://doi.org/10.3846/13923730.2012.720934.
[21] B. Benmokrane, V. Brown, K. Mohamed, A. Nanni, M. Rossini, C. Shield, Creep rupture limit for GFRP bars subjected to sustained loads, ASCE Journal of Composites for Construction 23 (6) (2019) 06019001. https://doi.org/10.1061/(ASCE)CC.1943-5614.0000971.
[22] EAD 260023-00-0301, Carbon, glass, basalt and aramid fibre reinforced polymer bars as reinforcement of structural elements. 2019, EOTA, OJ Publication: Decision (EU) 2024/1944.
[23] ISO/TC 71/SC 6 Non-traditional reinforcing materials for concrete structures, ISO 10406-1. Fibre-reinforced polymer (FRP) reinforcement of concrete - Test methods - Part 1: FRP bars and grids, 2015.
[24] L. Torres, K. Neocleous, K. Pilakoutas, Design procedure and simplified equations for the flexural capacity of concrete members reinforced with fibre-reinforced polymer bars, *fib* Structural Concrete 13 (2) (2012) 119 – 129. https://doi.org/10.1002/suco.201100045.
[25] C.E. Ospina, C.E. Bakis, Indirect flexural crack control of concrete beams and one-way slabs reinforced with FRP bars, in: T. Triantafillou (Eds.), 8th International Symposium on Fiber Reinforced Polymer Reinforcement for Concrete Structures (FRPRCS-8), University of Patras, 2007.
[26] R. J. Frosch, Another look at cracking and crack control in reinforced concrete, ACI Structural Journal 96 (3) (1999) 437-442. https://doi.org/ 10.14359/679.
[27] P. Bischoff, Computing deflections using ACI CODE-318-19 and beyond, Part 1, Concrete International 47 (2) (2025) 47-50.
[28] *fib* Bulletin 114, Serviceability Limit State of Concrete Structures - Background Document of *fib* MC2020, International Federation for Structural Concrete, *fib*. Lausanne, Switzerland, 2024.
[29] C. Miàs, L. Torres, A. Turon, C. Barris, Experimental study of immediate and time-dependent deflections of GFRP reinforced concrete beams, Composite Structures 96 (2013) 279–285. https://doi.org/10.1016/j.compstruct.2012.08.052.

[30] L. Torres, C. Miàs, A. Turon, M. Baena, A rational method to predict long-term deflections of FRP reinforced concrete members, Engineering Structures 40 (2012) 230–239. https://doi.org/10.1016/j.engstruct.2012.02.021.
[31] V. Brown, Sustained load deflections in GFRP reinforced concrete beams. In: Proceedings of the 3rd International Symposium on Non-Metallic (FRP) Reinforcement for Concrete Structures (FRPRCS-3) V. 2, pp. 495-502, Japan Concrete Institute, Japan,1997.
[32] P. Bischoff, L. Torres, Rational approach for computing long-term deflection of reinforced concrete. ACI Structural Journal 118 (2) (2021) 215-224. https://doi.org/10.14359/51728192.
[33] G. L. Balázs et al., Design for SLS according to fib Model Code 2010, *fib* Structural Concrete, 14 (2) (2013) 99-123. https://doi.org/10.1002/suco.201200060.
[34] T. Hall, A. Ghali, Long-term deflection prediction of concrete members reinforced with glass fibre reinforced polymer bars, Canadian Journal of Civil Engineering 27 (5) (2000) 890–8. https://doi.org/10.1139/l00-009.
[35] I.G. Gilbert, G. Ranzi, Time-Dependent Behaviour of Concrete Structures, CRC Press, London, UK, 2011.
[36] CEN, Eurocode – Basis of structural and geotechnical design – Part1: New structures (prEN 1990-1:2023), European Committee for Standardization, Brussels, Belgium, 2023.
[37] Comité Euro-International du Béton (CEB), CEB-FIP Model Code 1990 (MC-90), Thomas Telford, London, UK 1993.
[38] CEN, Eurocode 2, Design of Concrete Structures - Part 1-1: General Rules and Rules for Buildings, European Standard EN 1992-1-1 (2004), European Committee for Standardization, Brussels, Belgium, 2004.
[39] A. C. Scordelis, Computer models for nonlinear analysis of reinforced and prestressed concrete structures, PCI Journal 29 (6) (1984) 116-135. https://doi.org/10.15554/pcij.11011984.116.135.
[40] A. Marí, Nonlinear geometric, material and time dependent analysis of three dimensional reinforced and prestressed concrete frames, Department of Civil Engineering, University of California, Berkeley, California, 1984.
[41] CEB Design Manual Cracking and Deformations, CEB Bulletin d'Information N.158, Lausanne, 1984.
[42] Y.J. Kang, A.C. Scordelis, Non-linear segmental analysis of reinforced and prestressed concrete bridges. In: Proceedings of the 3rd International Conference on Short and Medium Span Bridges, pp. 229–240, Canadian Society for Civil Engineering, Montreal, Canada, 1990.
[43] P. Cruz, A. Marí, P. Roca, Nonlinear time-dependent analysis of segmentally constructed structures, ASCE Journal of Structural Engineering 124 (3) (1998) 278-287. https://doi.org/10.1061/(ASCE)0733-9445(1998)124:3(278).
[44] A. Marí, Numerical simulation of the segmental construction of three dimensional concrete frames, Engineering Structures 22 (6) (2000) 585-596. https://doi.org/10.1016/S0141-0296(99)00009-7.
[45] *fib* Bulletin 92, Serviceability Limit State of Concrete Structures, International Federation for Structural Concrete, *fib*. Lausanne, Switzerland, 2019.
[46] M.M. Elbadry, A. Ghali, Analysis of time-dependent effects in concrete structures using conventional linear computer programs, Canadian Journal of Civil Engineering 28 (2001) 190-200. https://doi.org/10.1139/l00-093.
[47] A. Ghali, R. Favre, M. Elbadry, Concrete structures. Stresses and deformation, third ed., London, UK, CRC Press, 2002.
[48] A. Marí, M. Valdés, Long-term behaviour of continuous precast concrete girder bridges model, ASCE Journal of Bridge Engineering 5 (1) (2000) 22-30. https://doi.org/10.1061/(ASCE)1084-0702(2000)5:1(22).
[49] A. Marí, J.M. Bairán, E. Oller, Assessment of the efficiency of strengthening solutions in concrete structures by means of non-linear step by step analysis models, Hormigón y Acero 72 (294/295) (2021) 59-75. https://doi.org/10.33586/hya.2021.3043.

[50] A. Marí, J.M. Bairán, E. Oller, N. Duarte, Modeling serviceability performance and ultimate capacity of corroded reinforced and prestressed concrete structures, *fib* Structural Concrete 23 (1) (2022) 6-15. https://doi.org/10.1002/suco.202100159.
[51] A. Ghali, M. Elbadry, User's manual and computer program CPF: Cracked plane frames in prestressed concrete, Research Report No. CE85-2, Department of Civil Engineering, University of Calgary, Calgary, AB, Canada, 1985.
[52] A. Scanlon, D.W. Murray, Time-dependent reinforced concrete slab deflections, ASCE Journal of the Structural Division 100 (9) (1974) 1911-1924. https://doi.org/10.1061/JSDEAG.0003881.
[53] R. I. Gilbert, R.F. Warner, Tension stiffening in reinforced concrete slabs, ASCE Journal of the Structural Division 104 (12) (1978) 1885-1900. https://doi.org/10.1061/JSDEAG.0005054.
[54] G. Kaklauskas, J Ghaboussi, Stress-strain relations for cracked tensile concrete from RC beam tests, ASCE Journal of Structural Engineering 127 (1) (2001) 64-73. https://doi.org/10.1061/(ASCE)0733-9445(2001)127:1(64).
[55] L. Torres, F. López-Almansa, L.M. Bozzo, Tension-stiffening model for cracked flexural concrete members, ASCE Journal of Structural Engineering 130 (8) (2004) 1242– 1251. https://doi.org/10.1061/(ASCE)0733-9445(2004)130:8(1242).
[56] A. Marí, J.M. Bairán, N. Duarte, Long-term deflections in cracked reinforced concrete flexural members, Engineering Structures 32 (3) (2010) 829-842. https://doi.org/10.1016/j.engstruct.2009.12.009.
[57] A. Marí, L. Torres, E. Oller, C. Barris, Performance-based slenderness limits for deformations and crack control of reinforced concrete flexural membres, Engineering Structures 187 (2019) 267-79. https://doi.org/10.1016/j.engstruct.2019.02.045.
[58] ACI 318-19, Building Code Requirements for Structural Concrete (ACI 318-19) and Commentary (ACI 318R-19), American Concrete Institute, ACI Committee 318, Farmington Hills, Michigan, USA, 2019.
[59] P. Bischoff, Comparison of existing approaches for computing deflections of reinforced concrete, ACI Structural Journal 117 (1) (2020) 231-240. https:/doi.org/ 10.14359/51718072
[60] P. Bischoff, S.P. Gross, Equivalent moment of inertia based on integration of curvature, ASCE Journal of Composites for Construction 15 (3) (2011) 263–273. https://doi.org/10.1061/(ASCE)CC.1943-5614.0000164.
[61] S. Walkup, E. Musselman, S. Gross, Effect of service load levels on long-term deflection multiplier, ACI Structural Journal 116 (2) (2019) 89-100. https://doi.org/ 10.14359/51711137.